BIOCHEMISTRY
including biophysical chemistry & molecular biology
Article

Biochemistry **2010,** *49,* 8873–8881 8873
DOI: 10.1021/bi1006546

The Oxygen-Tolerant Hydrogenase I from *Aquifex aeolicus* Weakly Interacts with Carbon Monoxide: An Electrochemical and Time-Resolved FTIR Study†

Maria-Eirini Pandelia,‡ Pascale Infossi,§ Marie Thérèse Giudici-Orticoni,§ and Wolfgang Lubitz*,‡

‡*Max-Planck-Institut für Bioanorganische Chemie, Stiftstrasse 34-36, Mülheim an der Ruhr D45470, Germany, and* §*Laboratoire de Bioénergétique et Ingénierie des Protéines, IMM-CNRS, 13402 Marseille, France*

Received April 28, 2010; Revised Manuscript Received August 27, 2010

ABSTRACT: The [NiFe] hydrogenase (Hase I) involved in the aerobic respiration of the hyperthermophilic bacterium *Aquifex aeolicus* shows increased oxygen tolerance and thermostability and can form very stable films on pyrolytic graphite electrodes. Oxygen-tolerant enzymes, like the ones from *A. aeolicus* and *Ralstonia eutropha*, are reported to be insensitive to CO inhibition. This is in contrast to known and well-characterized (oxygen-sensitive) hydrogenases, for which carbon monoxide is a competitive inhibitor. In this study, the interaction of Hase I from *A. aeolicus* with CO is examined using *in situ* infrared electrochemistry and time-resolved FTIR spectroscopy. We could observe the formation of a CO adduct state, a finding that set the grounds to investigate the affinity of an O_2-tolerant enzyme for binding CO as well as the reversibility of this process. In the case of *A. aeolicus*, this extrinsic CO is shown to be weakly attached and the adduct state is light-sensitive at low temperatures. The energetic parameters for the rebinding of CO at the active site were estimated from the rate constants of this process after photolysis and the results compared to those obtained for standard hydrogenases. Formation of a weak Ni−CO bond in the active site of Hase I most likely results from the different interaction of this enzyme with inhibitors and/or different active site electronic properties to which non standard amino acid residues in the vicinity of the active site might contribute.

Hydrogenases are metalloenzymes that couple oxidation of dihydrogen to the activity of redox-related partners according to the reaction (*1*) $H_2 \rightleftharpoons 2H^+ + 2e^-$. They are classified on the basis of their metal content into three distinct classes: [NiFe], [FeFe], and [Fe] or iron−sulfur cluster-free hydrogenases (Hmd). Structural information for representatives of all three classes has been obtained (*2*−*5*). They are widespread in prokaryotic and eukaryotic microorganisms, in which they play a pivotal role in their metabolic processes (*6*, *7*). These enzymes are also found in hyperthermophilic microbes (*7*) such as *Aquifex aeolicus*, which is a microaerobic, obligate chemolithoautotrophic bacterium (*8*). It is most commonly found in volcanic submarine waters and grows optimally between 85 and 95 °C. Its complete genome has been sequenced (*9*) and was found to encode three distinct [NiFe] hydrogenases (*10*). Among these enzymes, the membrane-bound hydrogenase I (Hase I) is involved in the aerobic respiration pathway with O_2 as the final electron acceptor (*10*, *11*). Hase I consists of two subunits (see Figure 1). The large subunit (∼70 kDa) contains the heterobimetallic nickel−iron site (see the inset of Figure 1). The active site is bound to the protein backbone by four cysteines, two of which are bridging the two metals. Fe is coordinated by two CN^- groups and one CO. An extra (bridging) ligand can occur depending on the redox state of the enzyme. The small subunit (∼40 kDa) contains the iron−sulfur centers that mediate the transfer of electrons between the [NiFe] site and the native electron acceptor, a diheme cytochrome *b*.

Hase I is particularly intriguing, due to its enhanced thermostability and oxygen tolerance (*12*−*14*). At room temperature and under atmospheric conditions, the as-isolated enzyme is found in an inactive form that in terms of standard hydrogenases can be associated with the readily activated Ni-B state (Ni^{3+}, paramagnetic $S = {}^1/_2$) (*10*, *15*). This species is known to carry a bridging hydroxide (OH^-) (*16*) between the two metal ions. In contrast to oxygen-sensitive hydrogenases, no signals corresponding to the slowly reactivated Ni-A state (*14*, *15*, *17*) could be observed in the as-isolated preparations of the enzyme. The presence of Ni-B and not Ni-A has been shown by electron paramagnetic resonance (EPR)[1] (*10*) and more recently by Fourier transform infrared (FTIR) spectroscopy studies (*14*).

One-electron reduction of Ni-B leads to the EPR-silent Ni-SIa state, without the inactive Ni-SI states as detectable intermediates (*14*, *18*) (see Schemes S1 and S2 of the Supporting Information) (*19*, *20*). Further reduction yields the active Ni-C state (Ni^{3+}, $S = {}^1/_2$). ENDOR and HYSCORE studies of the deuterated form of Ni-C have recently detected a hydride bound to the active site (*20*), consistent with previous studies on *Ralstonia eutropha* (*21*) and *Desulfovibrio vulgaris* Miyazaki (M) F (*22*, *23*). This hydride ligand is dissociated as a proton (*24*) upon illumination at cryogenic temperatures, leaving the enzyme in the Ni-L state(s) (*23*, *25*). One-electron reduction of Ni-C leads to the most reduced intermediate of the catalytic cycle termed Ni-R.[2] Only one Ni-R state has been observed for Hase I of *A. aeolicus* in the pH

†Supported by EU/Energy Network Project SOLAR-H2 (FP7 Contract 212508), BMBF (03SF0318B and 03SF0355C), Max-Planck Society, CNRS, ANR, the city of Marseilles, Région Provence-Alpes-Côte d'Azur, and "Pôle de compétitivité CapEnergies.

*To whom correspondence should be addressed. Phone: +49 (0)208 306-3614. Fax: +49 (0)208 306-3955. E-mail: lubitz@mpi-muelheim.mpg.de.

[1]Abbreviations: EPR, electron paramagnetic resonance; FTIR, Fourier transform infrared spectroscopy; PFE, protein film electrochemistry; PDB, Protein Data Bank.

[2]The "standard" Ni-R state in *A. aeolicus* resembles closely the Ni-R2 form of other oxygen-sensitive enzymes. For the sake of simplicity, we refer to this state as Ni-R in this work and avoid the numbering.

Published on Web 09/04/2010

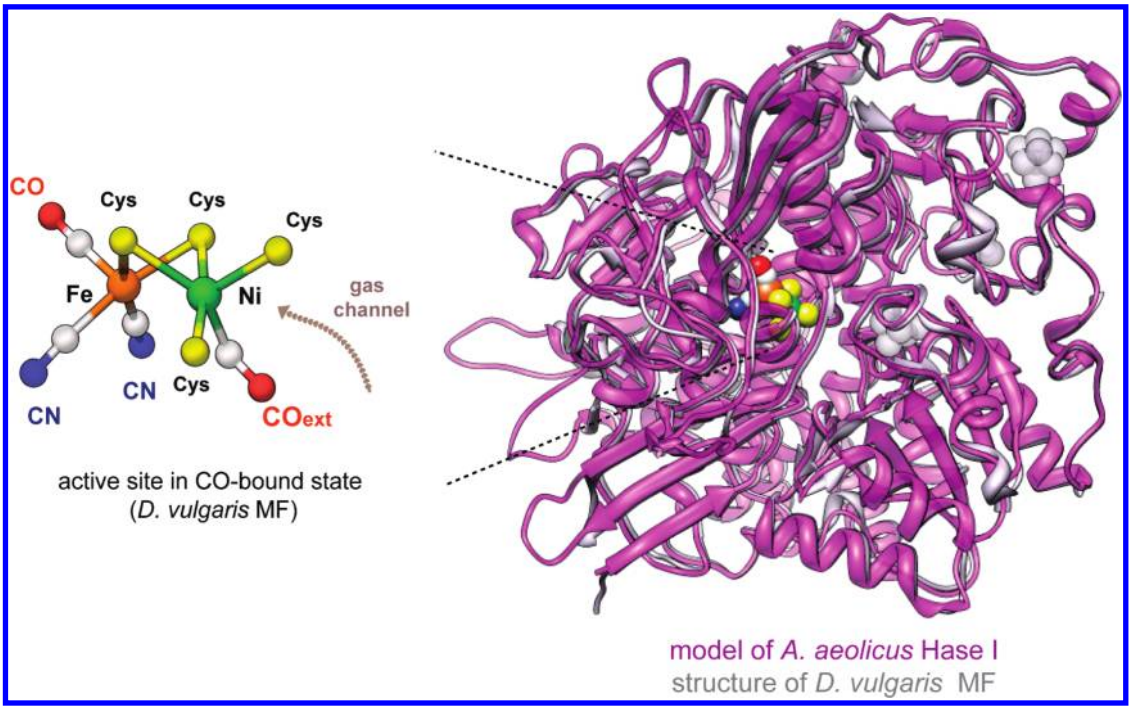

FIGURE 1: Homology model based on the amino acid sequence of the Hase I from *A. aeolicus* (purple) overlaid with the crystal structure of the *Desulfovibrio vulgaris* MF hydrogenase (gray, Protein Data Bank entry 1WUJ). The [FeS] clusters are colored gray. The enlarged inset at the left shows the [NiFe] site in the Ni-SCO inhibited state of the *D. vulgaris* MF (Protein Data Bank entry 1UBJ). The external carbon monoxide binds terminally to the open coordination site at the nickel near which the hydrophobic gas channel ends. A similar structure is assumed in the case of the *A. aeolicus* enzyme for the CO-bound structure.

range of 6.4−8.4 (*14*), in contrast to the three Ni-R forms reported for standard hydrogenases (*26*, *27*).

It has long been known that carbon monoxide inhibits the function of oxygen-sensitive hydrogenases (*28*, *29*). Infrared spectroscopic studies showed that this exogenous carbonyl binds to the nickel ion (*30*), which was later corroborated by X-ray crystallographic experiments (*31*) (see the inset of Figure 1). Such an inhibition can be reversed either by removal of CO from the protein solution or by illumination at cryogenic temperatures (*30*). For the Hase I from *A. aeolicus*, however, recent protein film electrochemistry (PFE) studies showed that in the presence of oxygen a significant enzymatic activity is retained, whereas no inhibition by carbon monoxide occurs (*13*, *14*). Such a finding is consistent with similar experiments with the oxygen-tolerant membrane-bound hydrogenase (MBH) from *R. eutropha* (*32*) and was attributed to the inability of such enzymes to bind carbon monoxide (*32*).

In this work, we demonstrate that O_2-tolerant enzymes such as *A. aeolicus* Hase I do form a CO adduct state; i.e., CO can access their active site and bind. A spectroscopic characterization of the CO-bound state of this oxygen-tolerant enzyme was carried out, and the results were compared with results for standard hydrogenases (*33*, *34*). The redox intermediates that bind CO were identified by *in situ* infrared electrochemistry with carbon monoxide in the solution (*33*, *34*). The activation barrier for the CO rebinding was estimated (*34*), taking advantage of the light sensitivity of the CO-bound state in a time-resolved FTIR kinetic study (*30*, *31*). The present findings should contribute to an improved understanding of the different reactions of the *A. aeolicus* Hase I with gaseous inhibitors (such as carbon monoxide) and may help establish a model for the molecular selectivity related to the oxygen tolerance of this enzyme.

MATERIALS AND METHODS

Protein Purification. Isolation and purification of the Hase I from *A. aeolicus* were carried out as previously described (*10*) in a 50 mM Tris-HCl buffer (pH 7.0) in the presence of 5−10% glycerol and 0.01% *n*-dodecyl β-D-maltoside (DDM).

Electrochemical Measurements. Electrochemical measurements in solution were taken in an Optically Transparent Thin-Layer Electrochemical (OTTLE) cell designed by Moss et al. (*35*, *36*). Twenty-five microliters of the protein-redox mediator solution was placed on a 8.5 μm thick gold (Au) mini-grid (70% transparent to infrared), which served as the working electrode. A platinum (Pt) foil was used as the counter electrode and a Ag/AgCl (1 M KCl) as the reference electrode. Calibration of the reference electrode prior to and after each measurement was performed by monitoring the reduction of methyl viologen (−448 mV, pH 7.0) with cyclic voltammetry. The temperature was regulated in the range between 4 and 40 °C by water passing through the metallic body of the cell in a closed external circuit with a thermostat (LAUDA).

The pH of the protein solution was kept at 7.4 in a 25 mM HEPES-NaOH buffer for all measurements. The titrations were carried out in the presence of the following redox mediating agents: methylviologen, benzylviologen, neutral red, phenosafranine, anthraquinone 2-sulfonate, anthraquinone 1,5-disulfonate, 2-hydroxy-1,4-naphthoquinone, potassium indigo tetrasulfonate, methylene blue, phenazine methosulfate, and naphthoquinone. Their redox potentials and pH dependence have been described previously (*37*, *38*). Additionally, KCl was added as an electrolyte to a final concentration of 100 mM. The final concentration of the mediators in the solution was 83 μM and that of the protein 180 μM. An equilibration time of 3−5 min was allowed prior to recording the infrared spectra at each potential (steady state). The potentiometric titrations were fitted in a

similar manner as described in ref *14*. All potentials mentioned in this work are quoted with respect to the normal hydrogen electrode potential (NHE).

Fourier Transform Infrared (FTIR) Spectroscopy. Infrared measurements were performed on a Bruker IFS 66v/s FTIR spectrometer with 2 cm^{-1} resolution. The detector was a photovoltaic mercury cadmium telluride (MCT) element. Time-resolved measurements at cryogenic temperatures were carried out in an Optistat CF cryostat with an ITC 503 temperature controller (Oxford Instruments). *In situ* illumination for 5 min was performed with a slide projector (250 W halogen lamp, 24 V) equipped with an electronic shutter (Compor). The low-temperature FTIR cell consists of two sapphire windows with an optical path length of 80 μm. The software for data recording consisted of the OPUS package (Bruker Optics). Analysis and further processing were performed with home-built routines written in MATLAB version 6.5 (Mathworks).

Sample Preparation and Treatment with Gases. For the electrochemical measurements, the solution consisting of Hase I and mediators was degassed prior to incubation for 30 min with carbon monoxide (N47, Air Liquide). The CO-saturated solution was subsequently transferred into the OTTLE cell under a 100% CO atmosphere in a glovebag.

For the low-temperature measurements, a 30 μL solution of 200 μM Hase I in 50 mM HEPES-NaOH (pH 7.4) was reduced with hydrogen gas (1.1 bar, N50, Air Liquide) for 30 min at room temperature and subsequently incubated for 30 min under 2.0 bar of CO (0 °C). In contrast to standard hydrogenases (e.g., *D. vulgaris* MF), longer incubation times under CO saturating conditions are required for the full inhibition of the enzyme.[3] The sample was transferred under anaerobic conditions in the FTIR cell and subsequently frozen in liquid nitrogen in the dark.

RESULTS

Infrared Electrochemistry in the Presence of CO. Figure 2a shows the FTIR spectrum of the as-isolated Hase I with CO in solution at a resting potential of +236 mV at 25 °C. Three bands can be observed in this spectrum, which are assigned to the stretching vibrations of the diatomic ligands coordinating the iron, one CO, and two CN^-. This spectrum corresponds to the inactive Ni-B state (see Table 1) (*14*). The more intense band at 1939 cm^{-1} is associated with the CO stretching vibration, while the two lower intensity bands at 2081 and 2092 cm^{-1} correspond to the coupled CN^- vibrations. In this work, the additional bands associated with a Ni-X state previously observed are absent from the spectrum (*14*); this is most likely related to the sample treatment. The yield of this state varies between different preparations, and its presence has been associated with an extra paramagnetic species corresponding to an oxidized state having a conformation different from Ni-B (*14*). Consistent with earlier observations on the standard hydrogenases, Hase I in the Ni-B state is not inhibited by CO (*33*, *34*, *39*).

Via application of a potential of −64 mV for 10 min, the FTIR spectrum in Figure 2b shows that the three intrinsic peaks are shifted to lower frequencies, while a fourth band at 2066 cm^{-1} has appeared. This is assigned to the extrinsic CO bound to nickel and clearly demonstrates that the enzyme interacts with carbon monoxide; Hase I is now entirely found in a CO-inhibited state. This state is EPR-silent (Ni^{2+}), as has been demonstrated by EPR

[3]Five minutes under 2.5 bar of CO for *D. vulgaris* MF (*34*) and 30 min under 2.0 bar of CO for *A. aeolicus* at 0 °C.

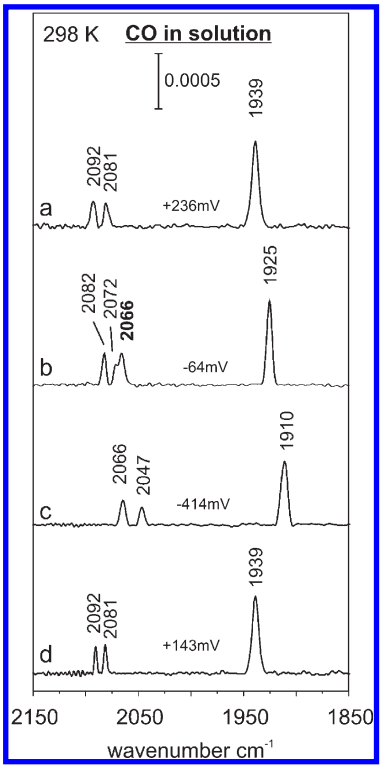

FIGURE 2: FTIR spectra of Hase I from *A. aeolicus* at 298 K in the presence of CO in solution. (a) At the resting potential of 236 mV, the as-isolated enzyme is in the Ni-B state. (b) At −64 mV, Ni-SCO has formed, as indicated by the fourth band at 2066 cm^{-1} (extrinsic CO). (c) At −414 mV, the extrinsic CO has been "disattached" and the enzyme is in the Ni-R state. (d) Reoxidation of the enzyme at 143 mV again yields the Ni-B state. Each spectrum is an average of 1000 scans with 2 cm^{-1} resolution.

Table 1: FTIR Stretching Vibrations Corresponding to the CO and CN^- Ligands of the Hase I from *A. aeolicus* for All Observed Intermediate States at 298 K[a]

state	$\bar{\nu}_{CO}$(Fe) (cm^{-1})	$\bar{\nu}_{CN^-}$(Fe)$_{asym}$ (cm^{-1})	$\bar{\nu}_{CN^-}$(Fe)$_{sym}$ (cm^{-1})	$\bar{\nu}_{CO}$(Ni) (cm^{-1})
Ni-B	1939 (1940)	2081 (2083)	2092 (2094)	–
Ni-SIa	1927 (1931)	2077 (2079)	2086 (2090)	–
Ni-C	1949 (1952)	2078 (2079)	2088 (2093)	–
Ni-R	1910	2047	2066	–
Ni-SCO (^{12}CO)	1925 (1927)	2072 (2074)	2082 (2086)	2066 (2072)
Ni-SCO (^{13}CO)	(1926)	(2073)	(2085)	(2026)

[a]Values in parentheses are for a temperature of 100 K. The error in the determination of the frequency bands is ±1 cm^{-1}. The values for the Ni-B and Ni-C states were taken from ref *14*.

(data not shown), and can thus be denoted as Ni-SCO following the nomenclature of standard hydrogenases (*33*, *34*). The bands corresponding to the intrinsic diatomic ligands to iron of the Ni-SCO state are shifted 2−4 cm^{-1} with respect to those of Ni-SIa (Table 1), in agreement with previous findings on standard hydrogenases (*33*, *34*).

Further lowering of the applied potential does not lead to any spectral changes until a potential of −274 mV is reached. At values more negative than −274 mV, however, the Ni-SCO signals are being replaced by the most reduced state, Ni-R. During this process, an electrochemical "cleavage" of the extrinsic CO takes place that is completed at −414 mV, in which all of the hydrogenase molecules are in the active Ni-R form (Figure 2c). The latter state is described by a CO band at 1910 cm^{-1} and a pair

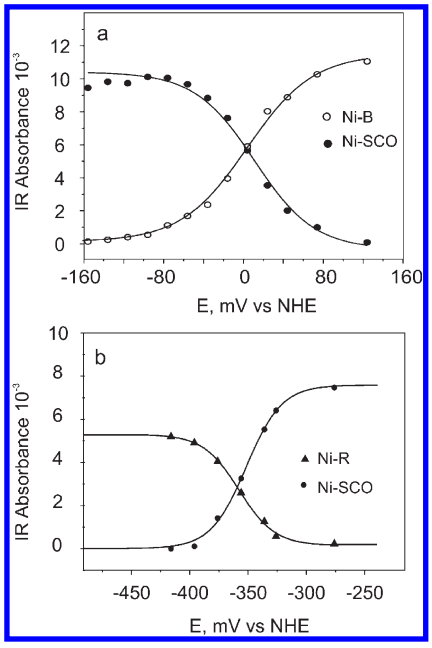

FIGURE 3: (a) Ni-B to Ni-SCO transition with an apparent midpoint potential (E_m) of -9 ± 10 mV corresponding to a single electron transfer. (b) Conversion of the Ni-SCO state to the Ni-R state could be described by a midpoint potential (E_m) of -358 ± 10 mV corresponding to a two-electron transition. Experimental conditions: 25 °C, resolution of 2 cm^{-1}, potential steps of 20 mV.

of cyanide bands at 2047 and 2066 cm^{-1}. At these negative redox potentials, Hase I has completely recovered from CO inhibition.

Subsequently, Hase I is stepwise reoxidized via application of more positive potentials in the electrochemical cell. All the spectral features mentioned above are reproduced, and at +143 mV, the enzyme returns completely to the Ni-B state (Figure 2d). This observation was unexpected, because in all hydrogenases studied so far, the Ni-SCO state is very resistant to oxidation under these experimental conditions (*33*, *34*). When reoxidation of Hase I is performed at 15 °C, the transition of the Ni-SCO state to the Ni-B state appears less favorable. At +143 mV and 15 °C, only 40% of the molecules were in the Ni-B state and the rest in the Ni-SCO state, as estimated from the integrated intensity of the respective CO bands (data not shown).

Potentiometric Titration in the Presence of Carbon Monoxide. The redox behavior of all three detectable states is depicted as a function of the redox poise in Figure 3. As the potential is lowered, the enzyme is being activated, resulting in a decrease of the Ni-B state and a concomitant increase of the Ni-SCO state in a range between +100 and −100 mV. The protein remains in the Ni-SCO state, and at values lower than −300 mV, the Ni-R state begins to form. At −414 mV, all of the hydrogenase molecules are found in the Ni-R active state.

Hase I, at 25 °C and depending on the potential, switches reversibly between the Ni-B and Ni-SCO states. This is in contrast to the case of standard hydrogenases, for which electrochemical reoxidation from Ni-SCO is irreversible (*33*, *34*). The potential dependence of the intensity of the infrared bands corresponding to the Ni-B and Ni-SCO states could be adequately approximated by the Nernst equation corresponding to a one-electron process; a formal midpoint potential (E_m) of -9 ± 10 mV was obtained. At potentials more negative than −80 mV, there was a constant slight decrease in the band intensities of the Ni-SCO state, whereas at potentials lower than −300 mV, a transition to the active Ni-R state occurred. This process could be described assuming a two-electron transfer and considering a midpoint potential of -358 ± 10 mV (Figure 3b).

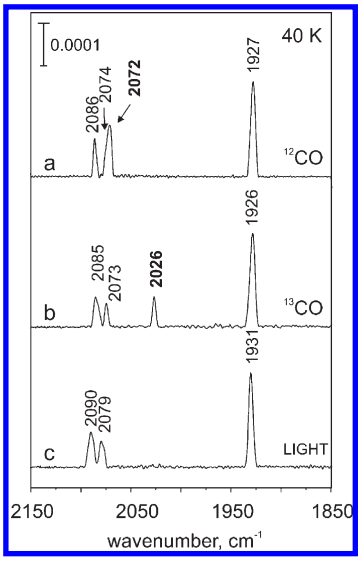

FIGURE 4: (a) FTIR spectra of the Ni-SCO state of Hase I from *A. aeolicus* at a cryogenic temperature (40 K) in the dark. The extrinsic CO is centered at 2072 cm^{-1}. (b) ^{13}CO isotope-labeled Ni-SCO state in the dark. The band corresponding to the exogenous CO is now shifted by 46 cm^{-1} to 2026 cm^{-1}. (c) Illuminated spectrum of the Ni-SCO state. The extrinsic CO is photodissociated, and the enzyme converts to the Ni-SIa state.

Low-Temperature FTIR and ^{13}CO Isotope Labeling. Figure 4a shows the FTIR spectrum of the CO-inhibited state (Ni-SCO) in Hase I at a low temperature (40 K). The infrared bands are now uniformly shifted by 0−4 cm^{-1} as compared to room-temperature measurements, because of the more restricted motion of the diatomic oscillators (*40*). The bands at 1927, 2074, and 2086 cm^{-1} are ascribed to the intrinsic CO and CN^- ligands. The fourth band at 2072 cm^{-1} is assigned to the extrinsically added carbon monoxide bound to nickel. Upon reaction of the active enzyme with isotope-labeled ^{13}CO, only the band of the exogenous carbonyl is expected to shift toward lower frequencies; the positions of all other bands remain the same, since they are uncoupled from the stretching vibration corresponding to the external CO. This is demonstrated in the spectrum of the ^{13}CO-inhibited Hase I at 40 K in Figure 4b. The absorption band of the extrinsic CO is shifted by 46 cm^{-1} and is now centered at 2026 cm^{-1}.

The Ni-SCO state is light-sensitive at cryogenic temperatures, consistent with earlier observations for other known hydrogenases (*30*, *31*, *34*). Illumination with white light at temperatures below 125 K leads to the disappearance of the band at 2072 cm^{-1} (^{12}CO) or 2026 cm^{-1} (^{13}CO) (Figure 4c), showing the photolytic loss of the externally added CO. The light-induced state formed corresponds to Ni-SIa. The bands of the intrinsic iron ligands are slightly shifted to higher frequencies compared to those of the Ni-SCO state, indicating a slight decrease in the electron density at the iron atom in the Ni-SIa state.

Kinetics and Activation Energy Barrier of the CO Rebinding in the Ni-SIa State. Conversion from Ni-SCO to the Ni-SIa state is reversible in the dark, involving dissociation of CO and its rebinding. In Figure 5a, the time evolution of a series of light-minus-dark difference spectra is shown in a three-dimensional representation at 112.5 K. The first slice of the spectrum corresponds to time zero ($t = 0$), where the amount of Ni-SIa is maximal. At subsequent times, the Ni-SCO state

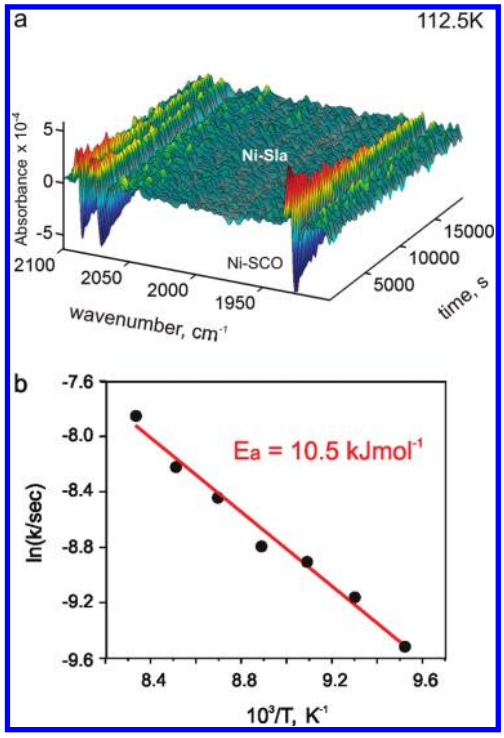

FIGURE 5: (a) Three-dimensional representation of a light-minus-dark difference infrared spectrum at 112.5 K. The disappearance of the bands corresponding to the Ni-SIa state (light product, positive signals) and the recovery of the Ni-SCO state (dark educt, negative signals) during dark adaptation is shown as a function of time. (b) Temperature dependence of the recombination rate constants. The activation energy barrier is given by the slope of the linear fit (Arrhenius).

reappears, as rebinding of CO to the active site occurs. The recombination rate constants were measured in a range between 120 and 105 K and have a single-exponential character indicating a first-order reaction.

The temperature dependence of the rate constants follows the empirical Arrhenius equation

$$k = A_0 \exp(-E_a/RT) \quad (1)$$

where k is the rate constant in inverse seconds, A_0 is the frequency factor in inverse seconds, E_a is the activation energy in kilojoules per mole, R is the universal gas constant (8.3144 J K^{-1} mol^{-1}), and T is the temperature in kelvin. The activation barrier for CO rebinding was estimated by analyzing the kinetics of the disappearance of Ni-SIa and the recovery of the Ni-SCO state, which were the same within experimental error (Figure 5b and Table 2). The lifetimes (inverse of the averaged rate constants) are given in Tables S1 and S2 of the Supporting Information for *A. aeolicus* and *D. vulgaris* MF, respectively. The activation barrier corresponds to ~10.5 kJ/mol, which is slightly larger than that found for *D. vulgaris* MF (*34*) (~8.0−9.2 kJ/mol).

The temperature dependence of the rate constants can be alternatively described in terms of the transition state theory (TST) that is expressed by the Eyring−Polanyi equation:

$$k_{TST} = \frac{k_B T}{h} \exp\left(\frac{\Delta S^{\ddagger}}{R}\right) \exp\left(-\frac{\Delta H^{\ddagger}}{RT}\right) \quad (2)$$

where $\Delta S^{\ddagger}$ and $\Delta H^{\ddagger}$ are the activation entropy and activation enthalpy, respectively (*41*). The activation entropy can be estimated from the intercept of the linear fit of the data plotted as $\ln(k_{TST}/T)$ as a function of $1/T$ (see Table 2). The activation entropy is found to be more negative in the case of *A. aeolicus*.

Table 2: Activation Energies, Frequency Factors, and Activation Entropies for the CO Rebinding in the Active Site of the Hase I from *A. aeolicus*[a]

species	E_a (kJ/mol)	A_0 (s^{-1})	$\Delta S^{\ddagger}$ (J mol^{-1} K^{-1})	$\Delta H^{\ddagger}$ (kJ/mol)
A. aeolicus				
single exponential	10.5	14	−224	9.6
D. vulgaris				
slow biexponential	8.8	500	−191	8.0
fast biexponential	8.0	2150	−179	7.3
single exponential	9.2	1800	−175	8.4

[a]The error in the calculated activation energies is 8%, in the frequency factors ~1 order of magnitude, and in the activation entropy 5%. Results for *D. vulgaris* MF (*34*) are included for comparison.

DISCUSSION

The Ni-SIa State Is the State That Binds CO. The as-isolated enzyme of Hase I is in the most oxidized Ni-B state (*10*, *14*). This state is spectroscopically very similar to that from mesophilic hydrogenases (*10*) and is thus also thought to carry a hydroxide ligand in its active site (*15*, *16*). In the presence of carbon monoxide in the protein solution of the as-isolated enzyme, all the hydrogenase molecules remain in the Ni-B state, showing that CO does not bind to this state. The oxidation state and electronic configuration (Ni^{3+}, d_{z^2}) of the complex as well as the presence of the oxygen-based bridging ligand are the reasons for hindering the binding of CO in Ni-B, similar to standard oxygen-sensitive hydrogenases (*33*, *34*).

Application of moderate negative potentials results in the activation of the enzyme by release of the oxygenic species and a first reduction of nickel to the 2+ oxidation state forming Ni-SIa. Carbon monoxide binds to the Hase I in this state, and the EPR-silent Ni-SCO state is formed (*33*, *34*). Similar to the case for known hydrogenases, the binding of CO to Ni-SIa results from the electronic configuration of this state, the ligand arrangement of the active site structure, and the presence of only a four-coordinated divalent nickel center (Ni^{2+}) (*34*).

Poising Hase I for 10 min at −64 mV is sufficient to convert the enzyme completely to the Ni-SCO state. This is in contrast to the case for *Desulfovibrio fructosovorans*, where the transition to the Ni-SCO state was achieved only after activation for 210 min at −249 mV (*33*). The potential for formation of the Ni-SCO state is approximately 200 mV more positive in Hase I compared to that in *D. fructosovorans* (−245 mV) (*33*) or *D. vulgaris* MF (−280 mV) (*34*). This deviation is not entirely clear, since reduction of the Ni-B state occurs at relatively similar potentials in both oxygen-tolerant and oxygen-sensitive hydrogenases. For Hase I, reduction of Ni-B in the presence of CO takes place at a more positive potential compared to that in the absence of CO (*14*). Considering the following relations, the CO binding constant (K_{CO}) for the active enzyme (Ni^{2+}) can be defined:

$$Ni^{3+} + e^- \rightleftharpoons Ni^{2+}$$

$$Ni^{2+} + CO \overset{K_{CO}}{\rightleftharpoons} Ni^{2+}-CO$$

The shift in the reduction potential of the Ni^{3+}/Ni^{2+} complex can then be determined by taking into account the Nernst equation (see eqs 3 and 4) (*42*, *43*)

$$E_m(CO) = E_m + \frac{RT}{F}(1 + K_{CO}[CO]) \quad (3)$$

or for 25 °C we have

$$E_m(CO) = E_m + 59 \log(K_{CO}[CO]) \quad \text{for} \quad K_{CO}[CO] \gg 1 \quad (4)$$

where $E_m(CO)$ is the apparent midpoint reduction potential of the complex in the presence of CO, E_m is the midpoint potential in the absence of CO, and [CO] is the carbon monoxide concentration. The upshift in the reduction potential observed is in agreement with earlier observations (*42*, *43*) and is dependent on the binding constant and on the concentration of CO. Since E_m increases with increasing CO concentration this indicates that CO binds more strongly to the reduced form (Ni^{2+}). Assuming now a similar CO concentration in both oxygen-tolerant and oxygen-sensitive enzymes and taking into account the larger shift in the apparent redox potential of Hase I, the binding constant of CO is suggested to be smaller in the latter (see eqs 3 and 4). This upshift in the values for the formation of Ni-SCO in Hase I may also be related to the absence of any detectable intermediates between the Ni-B and Ni-SIa states (see Scheme S2 of the Supporting Information) (*14*, *19*).

CO Binds More Weakly to Hase I. In this work, we demonstrate that CO can form a bond with the nickel site of Hase I, showing that carbon monoxide has both access and affinity to bind at the active center of this enzyme. Previous electrochemical studies, however, reached the opposite conclusion for oxygen-tolerant enzymes, including *A. aeolicus*, based on the absence of inhibition as reflected in the catalytic current (*13*, *32*). This apparent discrepancy remains to be elucidated and could be related to differences in the experimental conditions between protein film electrochemistry and solution assayed electrochemical experiments that differ with respect to the kinetics of CO binding and dissociation. CO inhibition is clearly observed for standard hydrogenases (*44*), whereas in the case of O_2, inhibition is detectable for both oxygen-sensitive and -tolerant enzymes (*14*, *32*, *44*).

The stretching vibration of the extrinsic CO in Hase I is centered at 2066 cm^{-1}, while in known hydrogenases (i.e., *Allochromatium vinosum*, *Desulfovibrio gigas*, *D. fructosovorans*, and *D. vulgaris* MF) (*27*, *30*, *34*), it appears at 2055−2056 cm^{-1}. The 10−11 cm^{-1} shift toward higher frequencies is indicative of a decrease in the extent of π-back-donation from the nickel to the carbon atom; CO thus binds more weakly in the active site of Hase I (*45*). ^{13}CO labeling shifts the extrinsic CO band by 46 cm^{-1} toward lower frequencies, in agreement with the theoretically predicted value for a "pure" CO vibration (*46*). Thus, the CKFF (Cotton Kraihanzel Force Field) (*45*) approximation can be used to calculate the stretching parameters. A force constant $k(^{12}CO)_{Aquifex}$ of 1730 N/m could be estimated.[4]. The higher force constant for CO compared to that of *D. vulgaris* MF [$k(^{12}CO)_{Desulfovibrio}$ = 1665 N/m] again shows a strengthening of the C−O bond and a concomitant weakening of the Ni−CO interaction in Hase I.

Redox Changes in the Presence of CO. Between −100 and −300 mV, Hase I remains in the CO-inhibited state, though the signal intensities slightly decrease. No shifts in the bands of Ni-SCO were detected in contrast to the cases of *D. fructosovorans* (*33*) and *D. vulgaris* MF (*34*), in which small shifts (1−3 cm^{-1}) were observed and associated with the reduction of the proximal [Fe_4S_4] cluster. On the basis of an electrochemical titration of the iron−sulfur centers of Hase I, the reduction potential for the proximal cluster was estimated to be +87 mV (*20*). The absence of changes in the FTIR spectra of the Ni-SCO state in Hase I can thus be explained, because at these potentials the proximal cluster is already reduced.

At potentials more negative than −300 mV, the extrinsic CO starts to dissociate, leading to the appearance of Ni-R, in which the coordination sphere of the Ni is presumably stabilized by the binding of a hydrogen molecule or a hydride ligand (*47*). A these potentials, the dissociation constant of CO increases more than the affinity of the Ni-SI state for carbon monoxide, which has previously been suggested (*44*). Electrochemical cleavage of CO has been observed to some extent in *D. fructosovorans* (*33*) and *D. vulgaris* MF (*34*), but at 200−300 mV more negative potentials. The reversible transition from Ni-SCO to Ni-R is a complex reaction that involves release of the extrinsic carbonyl and a series of redox steps of the complex that may also comprise binding of a hydrogenic ligand. For Hase I, this transition could be approximated by a two-electron process, considering it "uncoupled" from the accompanying chemical reactions. Such a simplified description is supported by the Nernst behavior (equilibrium) of the respective transitions and has an apparent midpoint potential of −358 mV.

The Ni-SCO state in the oxygen-sensitive hydrogenases is extremely resistant to electrochemical oxidation. Application of very positive redox potentials does not yield Ni-B; Ni-SCO persists (*33*, *34*). The situation in the *A. aeolicus* enzyme, however, is markedly different. Already, at −9 mV, the enzyme is in a mixture of equivalent amounts of Ni-SCO and Ni-B. This shows that the externally added CO can be easily displaced upon oxidation and Ni-B can be formed, most likely via insertion of an OH^- ligand from the solvent (anaerobic inactivation) (*17*). Both CO and oxygen inhibition are selectively tuned by changing the redox potential, which indicates competing processes, a weaker interaction of the active site with the extrinsic carbon monoxide and likely with the oxygen-based ligand compared to standard hydrogenases. The reversible transition from Ni-B to Ni-SCO involves release of the oxygen-based ligand, reduction of the nickel center, and binding of carbon monoxide and can be phenomenologically described as a single-electron transfer.

Kinetics and Energetics of the CO Rebinding after Photolysis. Illumination with white light at cryogenic temperatures results in the photolytic loss of the extrinsic CO and the appearance of the Ni-SIa state, showing that this is the state that binds the extrinsic carbonyl (*30*, *34*). A comparison of the activation barriers for the reassociation of CO between Hase I and oxygen-sensitive enzymes (e.g., *D. vulgaris* MF) (*34*) shows that these are very similar. On the other hand, the kinetics of this process for these two types of enzymes are very different; CO rebinds much slower to the active site of Hase I compared to that of *D. vulgaris* MF. The temperature range for the ligand recombination is not the same; however, considering the kinetics for the highest temperature at which cleavage of CO occurs, the CO rebinding rates in *A. aeolicus* are ~50 times slower. At lower temperatures, this difference becomes smaller (~12 times), but the value remains 1 order of magnitude larger, as reflected in the frequency factor A_0 (see the Supporting Information).

The nature of the activation energy barrier in a protein environment as well as the pre-exponential factor A_0 in the Arrhenius equation is difficult to precisely characterize, because in proteins there are a number of effects that can influence the rebinding kinetics of a ligand. For Hase I, the smaller frequency

[4]The force constant of the C−O bond is given by the equation $k(^{12}CO) = 4.0383 \times 10^{-4}\ \bar{\nu}^2$. For the free CO, the force constant k equals 1875 N/m.

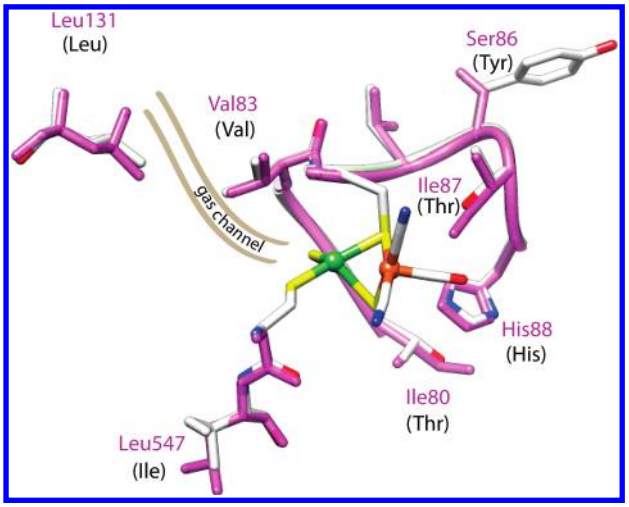

FIGURE 6: Homology model of Hase I constructed on the basis of the crystal structure of the Ni-B state from *D. vulgaris* MF (PDB entry 1WUJ). Both structures were aligned using the Swiss Pdb viewer package. The modeled structure of Hase I from *A. aeolicus* is colored purple. The numbering of the residues is based on the *D. vulgaris* MF numbering. The two nonconserved residues approximately 5 Å from the two metal ions are Ser86 and Ile87.

factor for this reaction is likely to be associated with a possible steric hindrance (orientation of the extrinsic carbonyl and/or conformation of the active site surrounding cavity) or with nonstandard residues in the vicinity of the [NiFe] site that would influence its electronic properties. The estimated activation entropy for *A. aeolicus* was shown to be more negative (Table 2) than that of *D. vulgaris* MF. This indicates that in Hase I the transition state (a state in which the carbon monoxide is quasi-bound) is more ordered with respect to the product state (Ni-SCO), resulting in a slower rate of the rebinding of CO. A larger barrier between the quasi-bound transition state and the final CO-bound complex would thus reveal a situation in which the protein conformation that facilitates binding of CO is induced at a slower rate (*48*). This may account for the absence of any CO inhibition in protein film electrochemistry experiments and may indicate that under physiological conditions the enzyme is not inhibited by CO.

To determine possible influences of the active site environment or steric hindrances, a homology model using the structure of PDB entry 1WUJ of *D. vulgaris* MF (Ni-B state) as a template was constructed. The residues shown are found within 10 Å of the bimetallic center (Figure 6). Two amino acid residues located in the vicinity of the active site (within approximately 5 Å of the two metal ions) are different from standard hydrogenases. For *D. vulgaris* MF, these residues are Tyr86 and Thr87, whereas in the sequence of *A. aeolicus* Hase I, these correspond to a serine and an isoleucine (Ser86 and Ile87, respectively, *D. vulgaris* numbering). For the oxygen-tolerant MBH from *R. eutropha*, the amino acids in these positions were found to be replaced instead with a glycine and a cysteine, respectively (*49*).

These specific residues are not located near the open coordination site of nickel, where the hydrophobic gas channel ends (Figure 6). For all three enzymes discussed, the amino acids that gate the hydrophobic gas channel near the open coordination site of the nickel, namely, Val83 and Leu131 (*D. vulgaris* MF numbering), are well-preserved (*49*). There is also no modification in the gas channel that has been observed for the oxygen-tolerant H_2-sensing hydrogenase from *R. eutropha* (RH) (*50*). Therefore, it is not considered likely that Ser and Ile in Hase I would directly affect the way gas molecules reach the active site. They could, however, influence the electronic and structural properties of the active site, resulting in a different reactivity with gaseous molecules.

In a recent study of the MBH from *R. eutropha*, these specific residues were mutated to probe their possible effect on the oxygen tolerance of the enzyme. When Gly86 (Ser86 in *A. aeolicus*) was replaced with a Tyr as in the case of the *Desulfovibrio* hydrogenases, this resulted in a loss of enzymatic activity, while substitution of Cys87 (Ile87 in *A. aeolicus*) had several implications but did not result in a significant oxygen sensitivity of the enzyme (*49*). These results demonstrate the importance of these residues for the stability of the [NiFe] center in oxygen-tolerant enzymes. A second study on *D. fructosovorans* engineered the inverse mutation, i.e., replaced the respective Thr and Tyr residues with the ones occurring in the MBH *R. eutropha* enzyme to examine their possible effect. Indeed, the H/D exchange activity was lowered, whereas the rate constants for binding and releasing CO were also decreased (*51*).

From this study, the different CO reassociation kinetics observed for *D. vulgaris* MF and *A. aeolicus* support the assumption that these residues are likely to be implicated in the transport or diffusion of gaseous molecules, by changing the conformation and polarity of the protein cavity surrounding. In addition, changes in the protein conformation and electrostatic environment are expected to alter the redox properties of the [NiFe] center and thus lead to a weaker interaction of the active site of Hase I with CO as reflected in the shift of the IR band of the extrinsic carbonyl. In general for other proteins, such as hemes, an increase in the stretching vibration frequency of the CO ligand has been associated with an increase in the reduction potential (*52*, *53*); this is in agreement with our observations described here.

SUMMARY

The active site of the oxygen-tolerant Hase I from *A. aeolicus* can react with carbon monoxide, however, under "stress conditions" involving long incubation times and saturating CO concentrations. Extrinsic CO can bind only to the active Ni-SIa state as a consequence of the electronic (Ni^{2+}) and structural configuration of the latter. The comparatively high stretching vibration frequency and large force constant of the exogenous carbonyl in the FTIR spectra of Hase I show that this ligand is bound only weakly to the active site. Unlike standard hydrogenases, the CO adduct can be reversibly reduced and reoxidized under loss of CO to Ni-R and Ni-B states, showing the versatility of this enzyme in switching between active and inactive forms in a comparatively small potential range. The energy barrier for the rebinding of CO after photolysis is comparable to that of *D. vulgaris* MF. The rebinding rate constants, frequency factor A_0, and the activation entropy are, however, different, suggesting an influence of the molecular environment on the interaction of the [NiFe] site with CO. We conclude that the enhanced tolerance of this enzyme toward gaseous inhibitors and in particular carbon monoxide is a synergetic effect combining formation of a weak Ni−CO bond and the presence of different amino acid residues in the vicinity of the active site. The role of these residues appears to be associated with electronic as well as entropic factors that influence the binding and release of CO and may lead to a more CO-tolerant and probably more O_2-tolerant hydrogenase.

ACKNOWLEDGMENT

We are grateful to Leslie J. Currell for technical support with the FTIR experiments, to Christophe Léger, Vincent Fourmond for the PFE measurements and helpful discussions and to Birgit Deckers for her help with the graphical artwork.

SUPPORTING INFORMATION AVAILABLE

Two tables with CO recombination lifetimes (inverse rate constants) for the *D. vulgaris* MF and *A. aeolicus* enzymes, one figure of the sequence alignment between the *D. vulgaris* MF and *A. aeolicus* Hase I large subunits, and two schemes related to the mechanism of standard and oxygen-sensitive hydrogenases. This material is available free of charge via the Internet at http://pubs.acs.org.

REFERENCES

1. Vignais, P. M., and Colbeau, A. (2004) Molecular biology of microbial hydrogenases. *Curr. Issues Mol. Biol. 6*, 159–188.
2. Vignais, P. M., and Billoud, B. (2007) Occurrence, classification, and biological function of hydrogenases: An overview. *Chem. Rev. 107*, 4206–4272.
3. Volbeda, A., Charon, M. H., Piras, C., Hatchikian, E. C., Frey, M., and Fontecilla-Camps, J. C. (1995) Crystal Structure of the Nickel-Iron Hydrogenase from *Desulfovibrio gigas*. *Nature 373*, 580–587.
4. Nicolet, Y., Lemon, B. J., Fontecilla-Camps, J. C., and Peters, J. W. (2000) A novel FeS cluster in Fe-only hydrogenases. *Trends Biochem. Sci. 25*, 138–143.
5. Shima, S., Pilak, O., Vogt, S., Schick, M., Stagni, M. S., Meyer-Klaucke, W., Warkentin, E., Thauer, R. K., and Ermler, U. (2008) The Crystal Structure of [Fe]-Hydrogenase Reveals the Geometry of the Active Site. *Science 321*, 572–575.
6. Dworkin, M., Falkow, S., Rosenberg, E., and Schleifer, K. H. (2007) The Prokaryotes: Ecophysiology and Biochemistry, 3rd ed., Vol. 2, Springer, New York.
7. Brock, T., Madigan, T., Martinko, J. M., and Parker, J. (1994) Biology of Microorganisms, 7th ed., Prentice-Hall International, Upper Saddle River, NJ.
8. Huber, R., Wilharm, T., Huber, D., Trincone, A., Burggraf, S., Konig, H., Rachel, R., Rockinger, I., Fricke, H., and Stetter, K. O. (1992) *Aquifex pyrophilus* gen. nov. sp. nov., represents a novel group of marine hyperthermophilic hydrogen-oxidizing bacteria. *Syst. Appl. Microbiol. 15*, 340–351.
9. Deckert, G., Warren, P. V., Gaasterland, T., Young, W. G., Lenox, A. L., Graham, D. E., Overbeek, R., Snead, M. A., Keller, M., Aujay, M., Huber, R., Feldman, R. A., Short, J. M., Olsen, G. J., and Swanson, R. V. (1998) The complete genome of the hyperthermophilic bacterium *Aquifex aeolicus*. *Nature 392*, 353–358.
10. Brugna-Guiral, M., Tron, P., Nitschke, W., Stetter, K. O., Burlat, B., Guigliarelli, B., Bruschi, M., and Giudici-Orticoni, M. T. (2003) [NiFe] hydrogenases from the hyperthermophilic bacterium *Aquifex aeolicus*: Properties, function, and phylogenetics. *Extremophiles 7*, 145–157.
11. Guiral, M., Prunetti, L., Lignon, S., Lebrun, R., Moinier, D., and Giudici-Orticoni, M. T. (2009) New Insights into the Respiratory Chains of the Chemolithoautotrophic and Hyperthermophilic Bacterium *Aquifex aeolicus*. *J. Proteome Res. 8*, 1717–1730.
12. Guiral, M., Tron, P., Belle, V., Aubert, C., Léger, C., Guigliarelli, B., and Giudici-Orticoni, M. T. (2006) Hyperthermostable and oxygen resistant hydrogenases from a hyperthermophilic bacterium *Aquifex aeolicus*: Physicochemical properties. *Int. J. Hydrogen Energy 31*, 1424–1431.
13. Luo, X., Brugna, M., Tron-Infossi, P., Giudici-Orticoni, M. T., and Lojou, E. (2009) Immobilization of the hyperthermophilic hydrogenase from *Aquifex aeolicus* bacterium onto gold and carbon nanotube electrodes for efficient H_2 oxidation. *J. Biol. Inorg. Chem. 14*, 1275–1288.
14. Pandelia, M. E., Fourmond, V., Tron-Infossi, P., Lojou, E., Bertrand, P., Léger, C., Giudici-Orticoni, M. T., and Lubitz, W. (2010) The Membrane-Bound Hydrogenase I from the Hyperthermophilic Bacterium *Aquifex aeolicus*: Enzyme Activation, Redox Intermediates and Oxygen Tolerance. *J. Am. Chem. Soc. 132*, 6991–7004.
15. Lubitz, W., Reijerse, E., and van Gastel, M. (2007) [NiFe] and [FeFe] hydrogenases studied by advanced magnetic resonance techniques. *Chem. Rev. 107*, 4331–4365.
16. van Gastel, M., Stein, M., Brecht, M., Schröder, O., Lendzian, F., Bittl, R., Ogata, H., Higuchi, Y., and Lubitz, W. (2006) A single-crystal ENDOR and density functional theory study of the oxidized states of the [NiFe] hydrogenase from *Desulfovibrio vulgaris* Miyazaki F. *J. Biol. Inorg. Chem. 11*, 41–51.
17. Lamle, S. E., Albracht, S. P. J., and Armstrong, F. A. (2004) Electrochemical Potential-Step Investigations of the Aerobic Interconversions of [NiFe]-Hydrogenase from *Allochromatium vinosum*: Insights into the Puzzling Difference between Unready and Ready Oxidized Inactive States. *J. Am. Chem. Soc. 126*, 14899–14909.
18. De Lacey, A. L., Hatchikian, E. C., Volbeda, A., Frey, M., Fontecilla-Camps, J. C., and Fernandez, V. M. (1997) Infrared spectroelectrochemical characterization of the [NiFe] hydrogenase of *Desulfovibrio gigas*. *J. Am. Chem. Soc. 119*, 7181–7189.
19. Pandelia, M. E., Ogata, H., and Lubitz, W. (2010) Intermediates in the Catalytic Cycle of [NiFe] Hydrogenase: Functional Spectroscopy of the Active Site. *ChemPhysChem 11*, 1127–1140.
20. Pandelia, M. E. (2009) [NiFe] hydrogenases from *Desulfovibrio vulgaris* Miyazaki F and *Aquifex aeolicus* studied by FTIR, EPR and electrochemical techniques: Redox intermediates, O_2/CO sensitivity and light-induced effects. Doctoral Thesis, Technical University Berlin, Berlin.
21. Brecht, M., van Gastel, M., Buhrke, T., Friedrich, B., and Lubitz, W. (2003) Direct detection of a hydrogen ligand in the [NiFe] center of the regulatory H_2-sensing hydrogenase from *Ralstonia eutropha* in its reduced state by HYSCORE and ENDOR spectroscopy. *J. Am. Chem. Soc. 125*, 13075–13083.
22. Foerster, S., van Gastel, M., Brecht, M., and Lubitz, W. (2005) An orientation-selected ENDOR and HYSCORE study of the Ni-C active state of *Desulfovibrio vulgaris* Miyazaki F hydrogenase. *J. Biol. Inorg. Chem. 10*, 51–62.
23. Foerster, S., Stein, M., Brecht, M., Ogata, H., Higuchi, Y., and Lubitz, W. (2003) Single crystal EPR studies of the reduced active site of [NiFe] hydrogenase from *Desulfovibrio vulgaris* Miyazaki F. *J. Am. Chem. Soc. 125*, 83–93.
24. Stein, M., van Lenthe, E., Baerends, E. J., and Lubitz, W. (2001) Relativistic DFT calculations of the paramagnetic intermediates of [NiFe] hydrogenase. Implications for the enzymatic mechanism. *J. Am. Chem. Soc. 123*, 5839–5840.
25. Albracht, S. P. J. (1994) Nickel Hydrogenases: In Search of the Active Site. *Biochim. Biophys. Acta 1188*, 167–204.
26. Fichtner, C., Laurich, C., Bothe, E., and Lubitz, W. (2006) Spectroelectrochemical characterization of the [NiFe] hydrogenase of *Desulfovibrio vulgaris* Miyazaki F. *Biochemistry 45*, 9706–9716.
27. De Lacey, A. L., Fernandez, V. M., Rousset, M., and Cammack, R. (2007) Activation and inactivation of hydrogenase function and the catalytic cycle: Spectroelectrochemical studies. *Chem. Rev. 107*, 4304–4330.
28. Purec, L., Krasna, A. I., and Rittenberg, D. (1962) The Inhibition of Hydrogenase by Carbon Monoxide and the Reversal of this Inhibition by Light. *Biochemistry 1*, 270–275.
29. van der Zwaan, J. W., Albracht, S. P. J., Fontijn, R. D., and Slater, E. C. (1985) EPR Evidence for Direct Interaction of Carbon-Monoxide with Nickel in Hydrogenase from *Chromatium vinosum*. *FEBS Lett. 179*, 271–277.
30. Bagley, K. A., van Garderen, C. J., Chen, M., Duin, E. C., Albracht, S. P. J., and Woodruff, W. H. (1994) Infrared Studies on the Interaction of Carbon-Monoxide with Divalent Nickel in Hydrogenase from *Chromatium vinosum*. *Biochemistry 33*, 9229–9236.
31. Ogata, H., Mizoguchi, Y., Mizuno, N., Miki, K., Adachi, S., Yasuoka, N., Yagi, T., Yamauchi, O., Hirota, S., and Higuchi, Y. (2002) Structural studies of the carbon monoxide complex of [NiFe]hydrogenase from *Desulfovibrio vulgaris* Miyazaki F: Suggestion for the initial activation site for dihydrogen. *J. Am. Chem. Soc. 124*, 11628–11635.
32. Vincent, K. A., Cracknell, J. A., Lenz, O., Zebger, I., Friedrich, B., and Armstrong, F. A. (2005) Electrocatalytic hydrogen oxidation by an enzyme at high carbon monoxide or oxygen levels. *Proc. Natl. Acad. Sci. U.S.A. 102*, 16951–16954.
33. De Lacey, A. L., Stadler, C., Fernandez, V. M., Hatchikian, E. C., Fan, H. J., Li, S. H., and Hall, M. B. (2002) IR spectroelectrochemical study of the binding of carbon monoxide to the active site of *Desulfovibrio fructosovorans* Ni-Fe hydrogenase. *J. Biol. Inorg. Chem. 7* (3), 318–326.
34. Pandelia, M. E., Ogata, H., Currell, L. J., Flores, M., and Lubitz, W. (2009) Inhibition of the [NiFe] Hydrogenase from *Desulfovibrio vulgaris* Miyazaki F by Carbon Monoxide: An FTIR and EPR Spectroscopic Study. *Biochim. Biophys. Acta 1797*, 304–313.
35. Moss, D. A., Leonhard, M., Bauscher, M., and Mantele, W. (1991) Electrochemical redox titration of cofactors in the reaction center from *Rhodobacter sphaeroides*. *FEBS Lett. 283*, 33–36.
36. Baymann, F., Moss, D. A., and Mantele, W. (1991) An Electrochemical Assay for the Characterization of Redox Proteins from Biological Electron-Transfer Chains. *Anal. Biochem. 199*, 269–274.
37. Fultz, M. L., and Durst, R. A. (1982) Mediator Compounds for the Electrochemical Study of Biological Redox Systems: A Compilation. *Anal. Chim. Acta 140*, 1–18.

38. Prince, R. C., Linkletter, S. J., and Dutton, P. L. (1981) The thermodynamic properties of some commonly used oxidation-reduction mediators, inhibitors and dyes, as determined by polarography. *Biochim. Biophys. Acta 635*, 132–148.
39. George, S. J., Kurkin, S., Thorneley, R. N. F., and Albracht, S. P. J. (2004) Reactions of H_2, CO, and O_2 with active [NiFe]-Hydrogenase from *Allochromatium vinosum*. A stopped-flow infrared study. *Biochemistry 43*, 6808–6819.
40. Nyquist, R. A. (1986) The Significance of Temperature and Solvent Effects upon Infrared Spectra and Group Frequencies. *Appl. Spectrosc. 40*, 79–85.
41. Laidler, K. J., and King, M. C. (1983) Development of transition-state theory. *J. Phys. Chem. 87*, 2657–2664.
42. Brzenzinski, P., and Wilson, M. (1997) Photochemical electron injection into redox active proteins. *Proc. Natl. Acad. Sci. U.S.A. 94*, 6176–6179.
43. Jung, H. J., Bang, H., and Suh, M. P. (2001) Carbon Monoxide Binding to Ni(I) Macrocyclic Complexes Generated by Electrochemical Method. *Bull. Korean Chem. Soc. 22*, 523–526.
44. Léger, C., Dementin, S., Bertrand, P., Rousset, M., and Guigliarelli, B. (2004) Inhibition and aerobic inactivation kinetics of *Desulfovibrio fructosovorans* NiFe hydrogenase studied by protein film voltammetry. *J. Am. Chem. Soc. 126*, 12162–12172.
45. Nakamoto, K. (1997) Infrared and Raman Spectra of Inorganic and Coordination Compounds, 5th ed., Vol. B, John Wiley & Sons, Inc., New York.
46. Braterman, P. S. (1975) Metal carbonyl spectra, Academic Press Inc., London.
47. Fontecilla-Camps, J. C., Amara, P., Cavazza, C., Nicolet, Y., and Volbeda, A. (2009) Structure-function relationships of anaerobic gas-processing metalloenzymes. *Nature 460*, 814–822.
48. Schramm, V. L. (1998) Enzymatic transition states and transition state analog design. *Annu. Rev. Biochem. 67*, 693–720.
49. Ludwig, M., Cracknell, J. A., Vincent, K. A., Armstrong, A. F., and Lenz, O. (2009) Oxygen-tolerant H_2 Oxidation by Membrane-bound [NiFe] Hydrogenases of *Ralstonia* Species: Coping with low levels of H_2 in AIR. *J. Biol. Chem. 284*, 465–477.
50. Buhrke, T., Lenz, O., Krauss, N., and Friedrich, B. (2005) Oxygen tolerance of the H_2-sensing [NiFe] hydrogenase from *Ralstonia eutropha* H16 is based on limited access of oxygen to the active site. *J. Biol. Chem. 280*, 23791–23796.
51. Leroux, F., Liebgott, P. P., Cournac, L., Richaud, P., Kpebe, A., Burlat, B., Guigliarelli, B., Bertand, P., Léger, C., Rousset, M., and Dementin, S. (2010) Is engineering O_2-tolerant hydrogenases just a matter of reproducing the active sites of the naturally occuring O_2-resistant enzymes? *Int. J. Hydrogen Energy* DOI: 10.1016/j.ijhydene.2010.02.071.
52. Smith, M. L., Paul, J., Ohlsson, P. I., and Paul, K. G. (1984) Correlations between Reduction Potential, CO Stretch Frequency and CO Half-Bandwidth in Hemoproteins. *Biochemistry 23*, 6776–6785.
53. Hershberger, J. W., and Kochi, J. K. (1983) Ligand effects on the redox potentials of metal carbonyls. *Polyhedron 2*, 929–934.